5-1-2010

CO and H+3 Toward MWC 1080, MWC 349, and LkHα 101

E L. Gibb
University of Missouri

Sean D. Brittain
Clemson University, sbritt@clemson.edu

T W. Rettig
University of Notre Dame

M Troutman
Clemson University

Theodore Simon
Eureka Scientific

See next page for additional authors

Authors

E L. Gibb, Sean D. Brittain, T W. Rettig, M Troutman, Theodore Simon, and C Kulesa

CO AND H_3^+ TOWARD MWC 1080, MWC 349, AND LkHα 101

E. L. GIBB[1], S. D. BRITTAIN[2], T. W. RETTIG[3], M. TROUTMAN[2], THEODORE SIMON[4], AND C. KULESA[5]
[1] Department of Physics & Astronomy, University of Missouri–St. Louis, St. Louis, MO 63121, USA
[2] Department of Physics & Astronomy, Clemson University, Clemson, SC 29634-0978, USA
[3] Center for Astrophysics, University of Notre Dame, Notre Dame, IN 46556, USA
[4] Eureka Scientific Inc., 1537 Kalaniwai Place, Honolulu, HI 96821, USA
[5] Steward Observatory, University of Arizona, 933 North Cherry Avenue, Tucson, AZ 85721, USA

ABSTRACT

We present high-resolution, near-infrared NIRSPEC observations of the fundamental rovibrational CO and H_3^+ R(1,0), R(1,1)^u, and Q(1,0) transitions toward three early-type young stars: MWC 1080, MWC 349, and LkHα 101. These observations were performed for the purpose of constraining the physical characteristics of the interstellar material along each line of sight. Toward MWC 1080, we detected strong CO absorption and determined a column density upper limit of 1.4×10^{14} cm^{-2} for H_3^+. We infer that there is very little diffuse material along the line of sight toward MWC 1080 and that the CO absorption is consistent with an origin in the dispersing natal cloud. We detected both cold CO and H_3^+ toward MWC 349, consistent with a diffuse cloud origin. Similarly, both CO and H_3^+ were detected toward LkHα 101. Using a recently revised value for the cosmic ray ionization rate, we conclude that the CO absorption is consistent with a dense cloud origin while the H_3^+ could originate in either the dense or diffuse interstellar medium. We also find no evidence for CO fractionation toward LkHα 101 as reported by Goto et al.

Key words: infrared: ISM – ISM: abundances – ISM: molecules – line: profiles

Online-only material: color figures

1. INTRODUCTION

In both dense and diffuse regions of the interstellar medium (ISM), CO is a common and easily observable molecule. H_2 is the most abundant molecule in the ISM but is difficult to observe because it is a homonuclear molecule and therefore has no dipole-allowed transitions. Thus, direct detection requires using the very weak quadrupolar transitions. It has been found that generally CO/$H_2 \sim 1.5 \times 10^{-4}$ in dense clouds (Lee et al. 1996) and $\sim 10^{-5}$–10^{-7} in diffuse clouds (Sheffer et al. 2008), making it useful as a diagnostic for H_2. Since the hydrogen column density can be estimated from the extinction (Mathis 1990), knowing the CO column densities and extinctions along the lines of sight to objects can assist in interpreting the nature of the interstellar material toward a background object like an early-type star.

H_3^+ is a molecule of fundamental importance to ion–molecule chemistry in the ISM. It has been observed in both the diffuse and dense ISM (McCall et al. 1998, 1999, 2002; Geballe et al. 1999). It is formed by cosmic ray ionization of H_2 into H_2^+, which then reacts rapidly with H_2 via the reaction $H_2^+ + H_2 \rightarrow H_3^+ + H$. In dense clouds the destruction of H_3^+ is dominated by reactions with CO, while in diffuse clouds electron recombination dominates the destruction. This relative simplicity in the formation and destruction mechanisms means that the abundance of H_3^+ can be used, in principle, to derive physical characteristics of the environments in which it is found, though this may be complicated by uncertainties in the H_2 ionization rate and the abundances of other species that, to a lesser extent, may contribute to the destruction of H_3^+ (Herbst 2000).

In this paper, we infer the nature and location of the interstellar material using high-resolution near-infrared H_3^+ and CO absorption spectroscopy toward three objects: MWC 1080, MWC 349, and LkHα 101. These are all young, early-type stars that have

rich emission line spectra and enough interstellar material to provide several magnitudes of visual extinction. In particular, we revisit the LkHα 101 results of Brittain et al. (2004) in which the analysis of three lines of H_3^+ in absorption led to the conclusion that the amount of diffuse material along the line of sight was insufficient to account for the observed H_3^+ column density. The recent work by Indriolo et al. (2007) implies a substantially higher cosmic ray ionization rate than assumed in earlier work, and we address whether this alters our earlier conclusions. Our observations and data reduction are discussed in Section 2, our analysis in Section 3. We discuss our results and interpretations in Section 4.

2. OBSERVATIONS AND DATA REDUCTION

The data presented herein were obtained with the high-dispersion, cross-dispersed, cryogenic echelle spectrometer NIRSPEC at the 10 m W. M. Keck Observatory on Mauna Kea, Hawaii (McLean et al. 1998). NIRSPEC has a 1024×1024 pixel InSb array detector that covers the 1–5.5 μm spectral region. A spectral resolving power of $\sim 25,000$ was obtained using the three-pixel (0.″43) slit. Absorption spectra of the fundamental branch of ^{12}CO and ^{13}CO in the *M* band were obtained for MWC 1080, MWC 349, and LkHα 101. In addition, we targeted the Q(1,0), R(1,0), and R(1,1)^u transitions of H_3^+ via two *KL* band settings toward the same three stars. The complete set of observations is summarized in Table 1.

All data were reduced using standard techniques, the details of which can be found in DiSanti et al. (2001) and Brittain et al. (2003). The infrared spectral region is dominated by telluric lines. To account for variations in atmospheric transmittance, we generated telluric models using the Spectral Synthesis Program (SSP; Kunde & Maguire 1974), which accesses the updated HITRAN 2004 database (Rothman et al. 2005). The telluric models were used for wavelength calibration and to determine

Table 1
Log of Observations

Source	Date	Spectral Coverage (cm^{-1})	Lines	Integration Time (minutes)
MWC 1080	2003 Nov 30	2746–2708	H$_3^+$ R(1,0), R(1,1)^u	12
		2533–2496	H$_3^+$ Q(1,0)	8
	2004 Jul 31	2018–1986, 2151–2117	CO (1–0)	16
MWC 349	2003 Aug 5	2746–2708	H$_3^+$ R(1,0), R(1,1)^u	12
		2533–2496	H$_3^+$ Q(1,0)	12
	2007 Jul 24	2018–1986, 2151–2117	CO (1–0)	4
LkHα 101	2002 Nov 15	2746–2708	H$_3^+$ R(1,0), R(1,1)^u	2
		2533–2496	H$_3^+$ Q(1,0)	2
	2003 Mar 17	2746–2708	H$_3^+$ R(1,0), R(1,1)^u	2
		2533–2496	H$_3^+$ Q(1,0)	2
	2003 Aug 12	2018–1986, 2151–2117	CO (1–0)	7
	2002 Nov 15	4320–4278, 4264–4220	CO (2–0)	8

column burdens for absorbing species in the atmosphere. The object spectrum is the residual difference between the extracted spectrum and the scaled telluric model (shown above the spectra in Figures 1–6). The *KL* settings exhibited a significant fringe, which we removed by deleting frequency spikes from the Fourier transform as described by Brittain et al. (2004).

3. ANALYSIS

Even with the resolving power of NIRSPEC (12 km s^{-1}), the narrow absorption features in our sources are unresolved. To determine the level populations of the CO from the combined, ratioed, and normalized spectra, we measured the equivalent width, $W_{\widetilde{\nu}}$, of each spectral line. We used two methods: (1) directly integrating over the line or (2) fitting a Gaussian to the line and calculating the integrated area. When possible, both measurements were performed to assess the validity of the computed uncertainties. Both methods gave comparable results for the integrated intensities. The uncertainty is given by the standard deviation of the continuum in the region surrounding the line position and is usually dominated by the quality of the telluric model fit.

3.1. CO Analysis

The sources presented in this work all exhibit fundamental ^{12}CO absorption lines. For an unsaturated CO line, the equivalent width (in cm^{-1}) is related to the column density in the lower state of the transition via

$$W_{\widetilde{\nu}} = \frac{\pi e^2}{mc^2} N_J f = 8.853 \times 10^{-13} N_J f.$$

In this equation, f denotes the absorption oscillator strength of the line, calculated from the tables in Goorvitch & Chackerian (1994). However, CO fundamental lines are usually optically thick. To correct the equivalent width for optical depth effects, we employed a curve-of-growth analysis (Spitzer 1978). In this case, the equivalent width is related to the optical depth as

$$W_{\widetilde{\nu}} = \int (1 - e^{-\tau}) d\widetilde{\nu},$$

where

$$\tau = \frac{\pi e^2}{mc^2} N_J f \Phi(\widetilde{\nu}),$$

and $\Phi(\widetilde{\nu})$ is the line shape function. If we assume the line is thermally broadened so that it follows a Maxwell-Boltzmann distribution, then

$$\Phi(\widetilde{\nu}) = \frac{\lambda_0}{\sqrt{\pi} b} e^{-v^2/b^2}.$$

The intrinsic line width is given by b (= $\sigma_{\rm rms}/1.665$, where $\sigma_{\rm rms}$ is the rms line width). Since our absorption lines are not resolved and we cannot measure b directly, we infer its value by considering the R and P branches separately. For example, the R1 and P1 lines probe the same energy level and should result in column densities that agree. Since they have different oscillator strengths, the line width can be adjusted until the level populations agree using

$$N_J = 66.8 \, b\widetilde{\nu} \, \tau_0 \, f.$$

We expect the low-J transitions to be thermalized when the CO is located in a circumstellar disk or dense interstellar cloud. In cases where CO absorption originates in diffuse material, the transitions may not be thermalized. This is the situation for MWC 349 (Section 4.2).

The ratioed residuals (corrected for transmittance) for MWC 1080, MWC 349, and LkHα 101 were fit with a model created from the relative CO rotational level populations (see Section 4). Rather than assuming that the CO rotation levels are thermalized, we calculated the population of the rotational levels of CO explicitly, following Warin et al. (1996). We assumed that the molecules were excited by a combination of collisional excitation and radiative pumping by the cosmic microwave background. For this calculation, only collisions with atomic hydrogen and H$_2$ were used, as they are the dominant collision partners. We adopted a ratio of H/H$_2$ = 0.5, though we note that varying H/H$_2$ between 0.1 and 1.0 only affects the final density by ~10%. When the model reaches a high density, the population approaches an LTE distribution. The collision rates were provided by the LAMDA online database, which uses rates from Wernli et al. (2006) and Flower & Pineau des Forêts (2001). The free parameters in the model are the column density of CO, the local hydrogen density, and the kinetic temperature of the collision partner(s). A suite of synthetic spectra was created with the three free parameters, and a chi-squared minimization of the model compared to the data was used to determine the best-fitting parameters. Our measured CO lines are presented
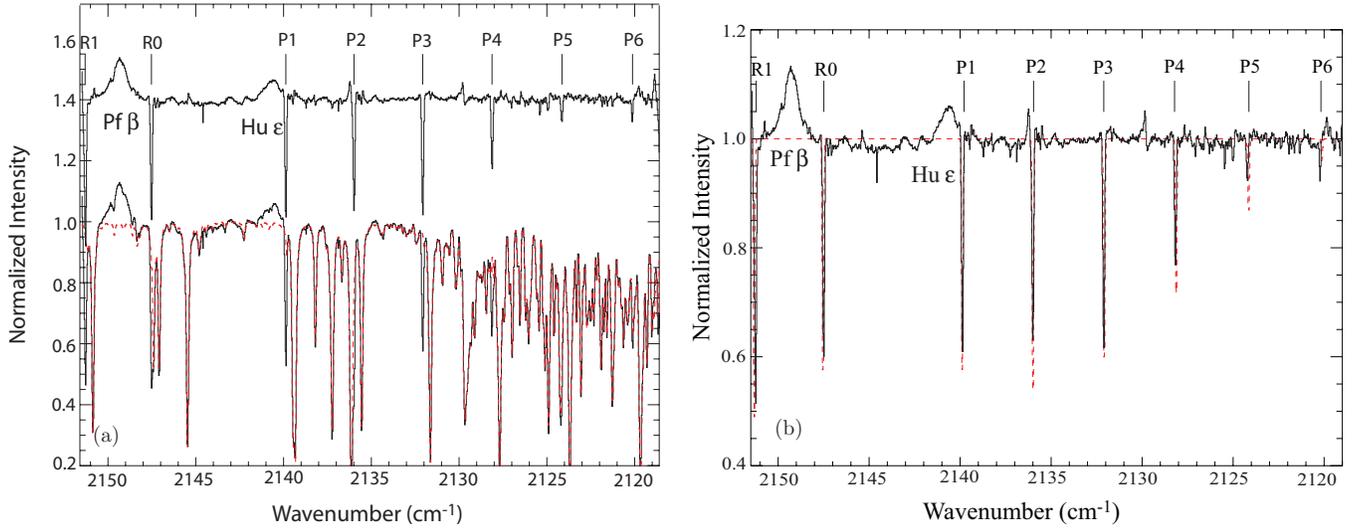
Figure 1. (a) Normalized *M*-band spectrum of MWC 1080. The red, dashed line overplotted is the telluric model. Plotted above the spectrum is the residual, the difference between the data and the model. The ^{12}CO (1–0) absorption lines are labeled (solid ticks) and are rapidly disappearing by P6. (b) Residual of MWC 1080, corrected for atmospheric transmittance (solid line) with the best-fit model overplotted (red dashed line, N(CO) $= 1.1 \times 10^{17}$ cm^{-2}, $T_{\rm rot} = 23$ K, $n_H > 10^5$ cm^{-3}) as discussed in Section 3.

(A color version of this figure is available in the online journal.)
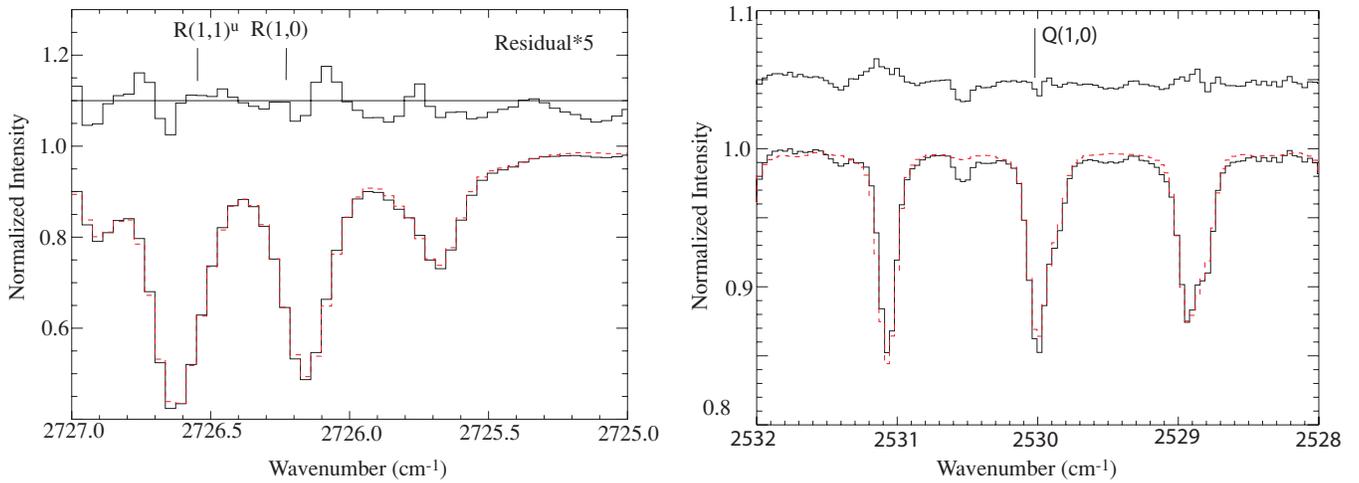

Figure 2. Normalized *L*-band spectra of MWC 1080 (solid line). The red, dashed line overplotted is the telluric model. Plotted above the spectrum is the residual, the difference between the data and the telluric model. For clarity, the residual has been multiplied by 5 for the R(1,1)^u and R(1,0) setting. The H$_3^+$ expected line positions are indicated by solid ticks.

(A color version of this figure is available in the online journal.)

in Tables 2–4. The results of our analysis for each source are presented in Section 4.

3.2. H$_3^+$ Analysis

H$_3^+$ has been studied in the laboratory since its initial laboratory detection (Oka 1980). A comprehensive line list is available in Lindsay & McCall (2001). With the advent of sensitive echelle spectrometers operating at infrared wavelengths, H$_3^+$ has now been detected toward many lines of sight and in a variety of interstellar environments from diffuse clouds to dense regions of star formation, with a fractional abundance of N(H$_3^+$)/$N_H \sim 2 \times 10^{-8}$ (e.g., Geballe et al. 1999; McCall et al. 2002).

The analysis is as follows. The column density for each transition of H$_3^+$ was calculated using

$$N\left(\mathrm{H}_3^+\right) = \frac{3hcW_{\tilde{\nu}}}{8\pi^3 \tilde{\nu}|\mu|^2},$$

where $\tilde{\nu}$ is the wavenumber and μ is the dipole moment of the transition (Lindsay & McCall 2001). The measured equivalent widths and resulting column densities of H$_3^+$ are given for each of the three stars in Table 5. At temperatures less than a few hundred Kelvin, only the (1,0) and (1,1)^u levels are populated. Since the Q(1,0) and R(1,0) transitions probe the same lower state and should result in the same column density, the total H$_3^+$ column density can be found by summing the contributions from the ($J = 1$, $K = 1$) and ($J = 1$, $K = 0$) states.

The R(1,0) and R(1,1)^u lines probe the ortho and para spin states, respectively, so we can in principle also calculate the excitation temperature of the gas from our data using

$$\frac{N_{\rm ortho}}{N_{\rm para}} = \frac{g_{\rm ortho}}{g_{\rm para}} e^{(-\Delta E/kT_{\rm ex})} = 2e^{(-32.87/T_{\rm ex})},$$

assuming that the gas is thermalized via either thermal collisions
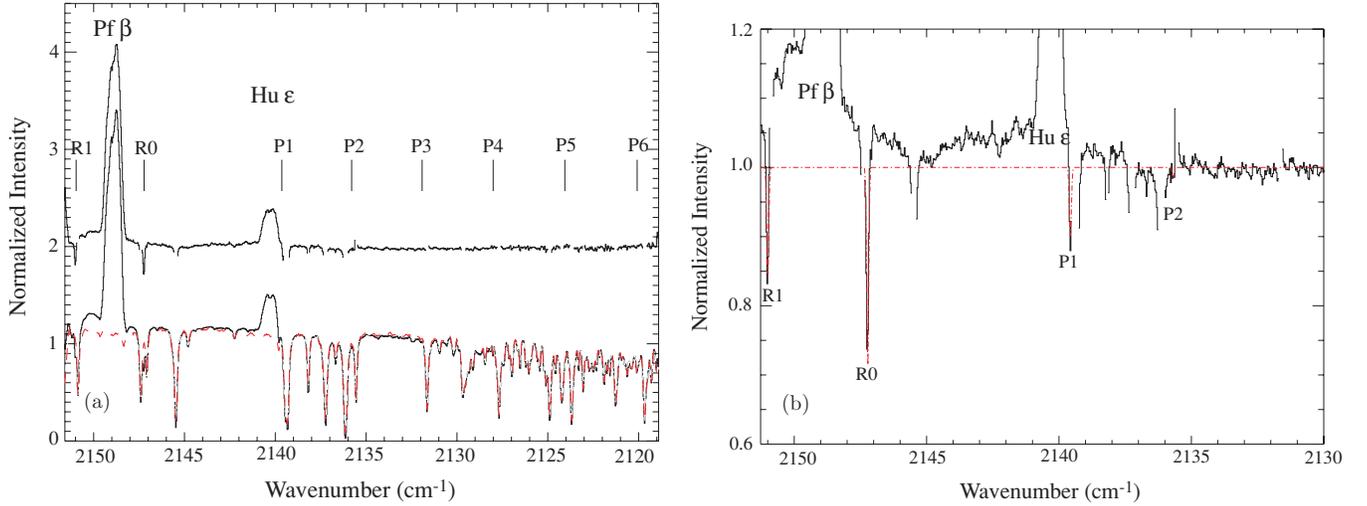
Figure 3. (a) Normalized M-band spectrum of MWC 349. The dashed line overplotted is the telluric model. Plotted above the spectrum is the residual, the difference between the data and the model. The ^{12}CO (1–0) absorption line positions are labeled (solid ticks) and are rapidly disappearing by P2. Gaps in the data indicate regions where the transmittance was <50% and were eliminated from the analysis. (b) Residual of MWC 349, corrected for atmospheric transmittance (solid line) with the best-fit model (red, dashed line, $N(CO) = 9.6 \times 10^{15}$ cm^{-2}, $T_{\rm rot} = 5$ K, $n_H = 250$ cm^{-3}) overplotted as discussed in Section 4.2.1.

(A color version of this figure is available in the online journal.)

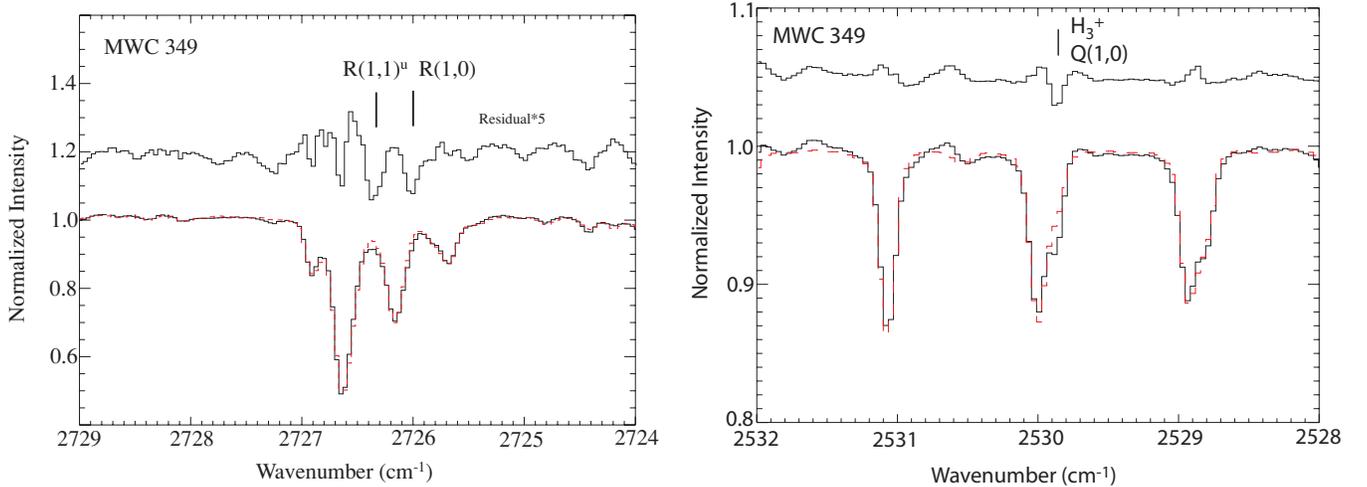**Figure 4.** Normalized L-band spectra of MWC 349 (solid line) showing the detection of the R(1,1)^u and R(1,0), and Q(1,0) lines of H$_3^+$. The telluric model is overplotted (dashed line). Plotted above is the residual, displaced vertically for clarity.

(A color version of this figure is available in the online journal.)

or proton exchange reactions with H$_2$. However, Indriolo et al. (2007) compared the excitation temperature for both H$_3^+$ and H$_2$ along several lines of sight and found the H$_2$ temperature, T_H, (typically about 60 K) to be consistently higher than that for H$_3^+$ ($\sim$30 K). We note that this is also consistent with the H$_2$ rotational temperature (77 ± 17 K) found in interstellar clouds with strong self-shielding by Savage et al. (1977). The reason for this discrepancy is not understood.

The production of H$_3^+$ in a diffuse cloud is determined by the cosmic ray ionization rate (ζ_2) and its destruction is determined by the e^- recombination rate. Hence,

$$\zeta_2 = N(H_3^+)\frac{k_e}{L}\frac{2}{f_2}\frac{n_e}{n_H} = 2.3\zeta_p, \qquad (1)$$

where ζ_2 is the ionization rate of molecular hydrogen (Glassgold & Langer 1974), ζ_p is the primary cosmic ray ionization rate (assumed to be 2×10^{-16} s^{-1} unless otherwise noted), L is the path length, f_2 is the molecular hydrogen fraction, and n_e and

n_H are the electron and hydrogen densities, respectively. In the diffuse ISM, f_2 has been inferred to be between $\sim$0.2 and 0.75 (Indriolo et al. 2007, and references therein), so we assume a value of 0.67 unless otherwise noted. We adopt the value of $n_e/n_H = 1.4 \times 10^{-4}$ found by Cardelli et al. (1996). k_e is given by

$$k_e = -1.3 \times 10^{-8} + 1.27 \times 10^{-6} \, T_e^{-0.48}$$

(McCall et al. 2004). Following Indriolo et al. (2007), in our analysis we assume $T_e = T_H = 60$ K rather than the $\sim$30 K excitation temperatures derived for H$_3^+$ as discussed above. Assuming $T_e = 30$ K would increase k$_e$ by $\sim$40%.

Some of our lines of sight sample the dense ISM. In the dense ISM, the destruction of H$_3^+$ is dominated by reactions with CO. Hence,

$$\zeta_2 = N(H_3^+)\frac{k_{CO}}{L}\frac{N(CO)}{N(H_2)}, \qquad (2)$$

where k_{CO} is the CO recombination rate, assumed to be 2×10^{-9} cm^3 s^{-1}. The canonical ionization rate, ζ_2, is 3×10^{-17} s^{-1}.
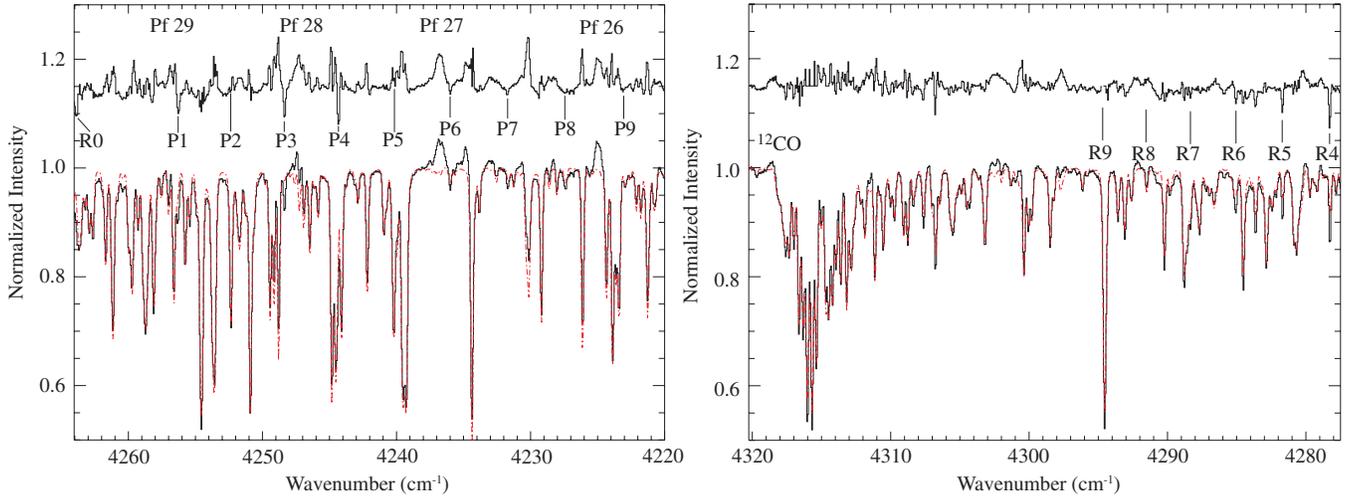
Figure 5. LkHα 101 *K*-band spectra showing the ^{12}CO overtone lines. The solid line is the spectrum. The red, dashed line is the telluric model. Plotted above the spectrum is the residual, displaced vertically for clarity. Positions of the ^{12}CO 2–0 lines are shown out to $J = 9$. Strong emission lines are due to atomic hydrogen.
(A color version of this figure is available in the online journal.)
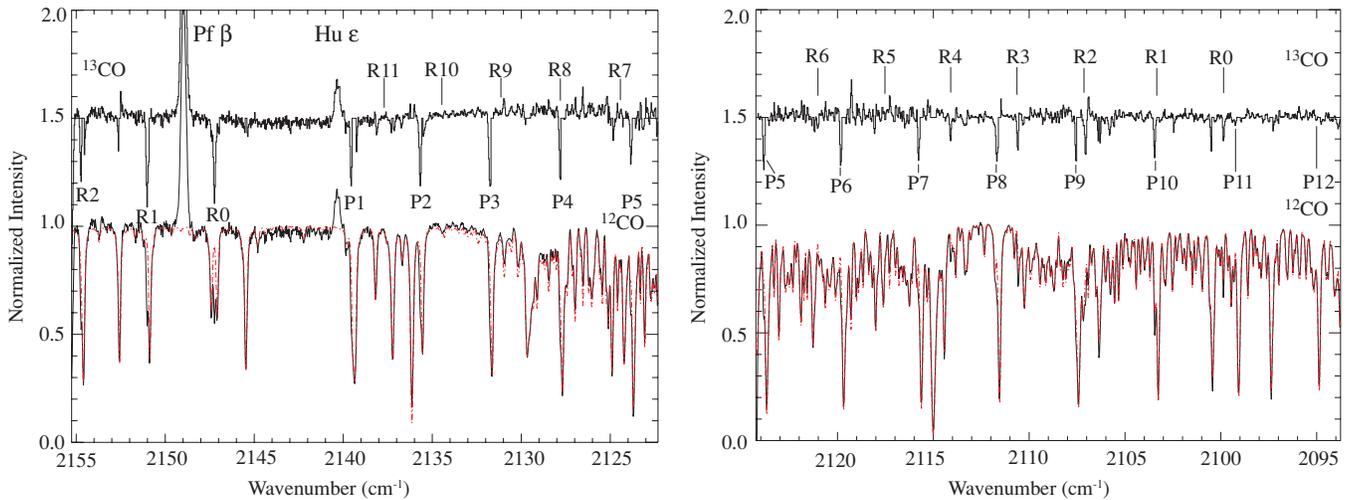

Figure 6. LkHα 101 *M*-band spectra showing the ^{12}CO (labeled below the residual) and ^{13}CO (labeled above the residual) fundamental absorption lines. The solid line is the spectrum. The red, dashed line is the telluric model. Plotted above the spectrum is the residual, displaced vertically for clarity. The strong emission lines near 2149 and 2141 cm^{-1} are due to hydrogen Pf β and Hu ϵ, respectively.
(A color version of this figure is available in the online journal.)

<div style="display:flex">
<div>

Table 2
^{12}CO (1–0) lines in MWC 1080

Line ID	$\widetilde{\nu}$ (cm^{-1})	$W_{\widetilde{\nu}}$ ($\times 10^{-3}$ cm^{-1})
R1	2151.28	66.4 ± 1.0
R0	2147.53	63.2 ± 1.2
P1	2139.87	52.1 ± 1.2
P2	2135.98	54.0 ± 1.4
P3	2132.07	46.1 ± 1.2
P4	2128.12	30.1 ± 1.3
P5	2124.15	17.1 ± 2.0
P6	2120.14	9.1 ± 1.5

</div>
<div>

Table 3
^{12}CO (1–0) lines in MWC 349

Line ID	$\widetilde{\nu}$ (cm^{-1})	$W_{\widetilde{\nu}}$ ($\times 10^{-3}$ cm^{-1})
R1	2150.86	33 ± 5
R0	2147.08	36 ± 10
P1	2139.43	15 ± 5
P2	2135.55	2 ± 2

</div>
</div>

4. RESULTS

4.1. MWC 1080

MWC 1080 is an intriguing young Herbig Ae/Be star in a cluster of forming stars that was first discovered by Merrill &

Burwell (1949). The spectral type is B0e according to Cohen & Kuhi (1979). Yoshida et al. (1992) assigned a much later spectral type of A0–A3 on the basis of optical spectroscopy. Estimates of the distance range from 2.2 kpc (Levreault 1985; Grankin et al. 1992) to 2.5 kpc (Cantó et al. 1984; Yoshida et al. 1992). It is known to be an eclipsing binary with a short (2.8869 day) period (Grankin et al. 1992; Schevchenko et al. 1994) and a circumbinary disk with a mass of ∼0.003 $M_\odot$ (Fuente et al. 2003). The visual extinction toward MWC 1080 is estimated to

Table 4
CO lines in LkHα 101

Molecule	Line ID	$\widetilde{\nu}$ (cm^{-1})	$W_{\widetilde{\nu}}$ ($\times 10^{-3}$ cm^{-1})
^{12}CO (2–0)	R10	4297.70	2.0 ± 0.4
	R8	4291.50	3.7 ± 0.5
	R7	4288.33	6.7 ± 1.0
	R6	4285.05	8.5 ± 0.6
	R5	4281.70	12.6 ± 0.5
	R4	4278.27	15.6 ± 0.4
	R0	4263.91	9 ± 1
	P1	4256.26	7 ± 1
	P3	4248.35	9 ± 1
	P4	4244.30	15.1 ± 1
	P5	4240.14	6 ± 2
	P6	4235.98	6.1 ± 1
	P7	4231.72	4.1 ± 0.4
	P8	4227.35	3.4 ± 0.4
	P9	4222.95	2.9 ± 0.4
	P11	4213.95	<2
	P12	4209.34	<0.9
^{13}CO (1–0)	R6	2121.01	3.0 ± 0.1
	R4	2114.10	10.2 ± 0.1
	R3	2110.59	13.9 ± 0.1
	R2	2107.05	14.8 ± 0.1
	R0	2099.86	11.3 ± 0.1
	P2	2088.83	13.9 ± 1.4
	P3	2085.09	8.0 ± 2
	P4	2081.31	8.7 ± 0.01
	P6	2073.67	5.0 ± 2.0

be 5.4 mag (Cohen & Kuhi 1979) or 4.4 mag (Yoshida et al. 1992), depending on the assumed spectral type and distance. Polarization measurements indicate that most of the extinction is likely due to interstellar material, the remaining $A_V \sim$ 1 mag arising from the circumstellar disk (Poetzel et al. 1992; Finkenzeller & Mundt 1984). It is associated with an optical outflow (Poetzel et al. 1992) and a bipolar CO outflow (Yoshida et al. 1991; Fuente et al. 1998). Recent BIMA observations show that the natal gas in the region is dispersing under the influence of MWC 1080 (Wang et al. 2008).

4.1.1. CO Toward MWC 1080

Figure 1(a) shows a high-resolution *M*-band spectrum of MWC 1080. Strong absorption lines of ^{12}CO (1–0) and weak ^{12}CO (2–1) emission lines are present. The emission lines are attributed to hot CO gas in the inner circumstellar disk of MWC 1080 and further analysis of them is beyond the scope of this paper. The strong, broad emission lines near 2149 cm^{-1} and 2141 cm^{-1} are due to hydrogen Pf β and Hu ε, respectively. The CO absorption lines are rapidly disappearing by P6, indicating a low rotational temperature.

Can we determine where along the line of sight the CO absorption originates? If the density of gas toward MWC 1080 is very low, CO may not be thermalized and could be said to originate in the diffuse ISM. If the CO is located in the denser circumstellar material, then the CO lines should be thermalized. Assuming no contribution above $J = 6$ and optically thin lines, we find the total ^{12}CO column density, N(CO), to be $\sim 5.6 \times 10^{16}$ cm^{-2}. Under this assumption, however, the P1 and R1 lines do not give the same column density. Alternatively, from a curve-of-growth analysis, we find $T_{\rm rot} \sim 23$ K and N(CO) $\sim 1.1 \times 10^{17}$ cm^{-2}. The CO column densities for the R1 and P1 lines agree for intrinsic Doppler widths between 3 and 4 km s^{-1}. The rotation analysis is linear and would seem to imply that the density of gas toward MWC 1080 is high enough for the CO to be thermalized, consistent with a location in a dense medium. Indeed, when we generate a best-fit synthetic spectrum using the model described in Section 3.1, shown in Figure 1(b), the best fit is for a density of $>10^5$ cm^{-3} and $T_{\rm rot} = 23$ K, consistent with thermalized cold, dense material. Hence, we adopt a total CO column density of 1.1×10^{17} cm^{-2}.

Applying the Bohlin et al. (1978) relation, $N_H/E(B-V) = 5.8 \times 10^{21}$ atoms cm^{-2} mag^{-1}, and assuming $A_V = 3.05$ $E(B-V)$, we can estimate the total gas column toward MWC 1080, $N_H = 8.4 \times 10^{21}$ atoms cm^{-2} (N(H$_2$) $= 4.2 \times 10^{21}$ if hydrogen is in molecular form) for ~ 4.4 mag of visual extinction. With N(CO) $= 1.1 \times 10^{17}$ cm^{-2} and $f_2 \sim 0.67$, the CO/H$_2$ ratio is 3.9×10^{-5}, somewhat less than the 1.5×10^{-4} found for dense clouds (Kulesa & Black 2003). However, the ionization rate can be expected to be higher, and thus the molecular hydrogen fraction lower, for material located in close proximity to an early-type star. This seems reasonable with moderately dense material being dispersed from the natal cloud by MWC 1080 (above).

The overall picture developing from the CO analysis is the presence of a small amount of hot CO in the disk around MWC 1080 with cold CO absorption from the dense, cold material out of which the cluster is forming. There appears to be very little diffuse interstellar material along the line of sight, consistent with the visual extinction toward MWC 1080.

4.1.2. H$_3^+$ Toward MWC 1080

The presence of strong, cold CO absorption lines toward MWC 1080 implies interstellar material, since as discussed above, the CO absorption is not consistent with a disk origin. We found from the CO absorption lines a Doppler shift of -63 km s^{-1} on July 31, corresponding to a geocentric Doppler shift of the absorbing gas of -36 km s^{-1} on November 30 (see Table 1). These are consistent with the reported heliocentric Doppler shift of -39 km s^{-1} (Levreault 1988), within a pixel of our estimated Doppler shift at the resolving power of our data. The fact that the ^{12}CO absorption lines are consistent with a very cold (~ 23 K) temperature argues that any H$_3^+$ formed in the same medium must populate the lowest levels, giving rise to the Q(1,0), R(1,1)^u, and R(1,0) transitions. We searched for but did not detect the R(1,0), R(1,1)^u and Q(1,0) lines of H$_3^+$ toward MWC 1080, assuming the same heliocentric Doppler shift for H$_3^+$ as found for the ^{12}CO absorption. The spectra are shown in Figure 2, and the expected Doppler shifted positions are indicated. We determined a 3σ column density upper limit of 1.4×10^{14} cm^{-2}. We can use this value and Equation (11) from Indriolo et al. (2007) to estimate the upper limit for the size of a diffuse cloud toward MWC 1080, which we find to be <6.8 pc, assuming a primary cosmic ray ionization rate of 2×10^{-16} s^{-1}. Since the CO analysis points to an origin in the dispersing circumstellar envelope, we can also calculate the size of a cloud of dense material assuming $k_{\rm CO} \sim 2 \times 10^{-9}$ cm^3 s^{-1}. We find a 3σ upper limit of 0.4 pc. We note that this could be a conservative estimate since close proximity to a B0 star would increase the ionization rate of H$_2$, decreasing the path length. The amount of dense material in the dispersing nebular material around MWC 1080 is too small to give rise to a significant column of H$_3^+$, consistent with our non-detection.

4.2. MWC 349

MWC 349A is an unusual B[e] star that displays characteristics of both a young stellar object and an evolved object. It is the brightest radio continuum star in the sky at 6 cm (Tafoya et al. 2004), is located in the direction of the Cyg OB2 association, and may have a binary companion, a B0 III star, located 2″.4 away (Merrill et al. 1932; Cohen et al. 1985). Radio continuum observations by Tafoya et al. (2004) support a connection between MWC 349A and MWC349B, implying that MWC 349A is an evolved B star as well. On the other hand, Meyer et al. (2002) argue that the arc of radio emission that apparently connects MWC 349A with nearby MWC 349B could be due to the complex background structure in that region. They suggest that MWC 349A is a young object and that the evolved MWC 349B is more distant and not associated with MWC 349A. Hofmann et al. (2002) argue that MWC 349A is a B[e] supergiant, similar to the evolved B[e] stars in the Magellanic Clouds, based on the spectral energy distribution, the lack of a 9.7 μm silicate feature, the existence of a fossil shell surrounding the system, and the emission line profiles. They argue that it is a member of the Cyg OB2 association at a distance of 1.7 kpc, though Cohen et al. (1985) estimated a distance of 1.2 kpc, which would preclude it being a member of the Cyg OB2 association.

4.2.1. CO Toward MWC 349A

We observed MWC 349A at the M band to study the fundamental CO lines (see Table 3). We detected CO gas in absorption only. As can be seen in Figure 3(a), the lowest $J'' = 0$-1 lines are quite strong, but the $J'' = 2$ and $J'' = 3$ lines are not observed, indicating that the gas is extremely cold, similar to the spectrum for Cyg OB2 No. 12 (McCall et al. 1998). If we assume that the CO is optically thin, we find $T_{\rm rot} \sim 5$ K and $N(\rm CO) = (9.6 \pm 2.7) \times 10^{15}$ cm^{-2}. This temperature is far too cold to be due to material in the disk, which is found to have a very warm temperature (Harvey et al. 1979). Such a cold $T_{\rm rot}$ in a diffuse cloud likely indicates that the CO has not been thermalized.

In Figure 3(b), we show the tellurically corrected residual. Overplotted is the synthetic spectrum derived using the model described in Section 3.1 with $n_H = 250$ cm^{-3} and $T_H = 60$ K, a typical hydrogen density and temperature in diffuse clouds. This model reproduces the CO absorption spectrum observed toward MWC 349, though we note that an equally good fit can be found with a higher density and lower hydrogen temperature ($n_H = 900$ cm^{-3} and $T_H = 23$ K).

Given the interstellar A_V of 8.9 mag, we estimate $N_H \sim 1.7 \times 10^{22}$ cm^{-2}, resulting in $N(\rm CO)/N_H \sim 6 \times 10^{-7}$, consistent with diffuse interstellar material subjected to ionizing radiation (van Dishoeck & Black 1988). Hence, we conclude that the CO absorption we detected originates in diffuse interstellar material.

4.2.2. H$_3^+$ Toward MWC 349A

As shown in Figure 4, we detected the R(1,1)^u and R(1,0) doublet and the Q(1,0) transitions of H$_3^+$ in absorption toward MWC 349A. The line equivalent widths and resulting column densities are shown in Table 5. We found $N(\rm H_3^+) = (3.9 \pm 1.3) \times 10^{14}$. The ortho-to-para ratio (0.3235) results in a $T_{\rm ex} \sim 22 \pm 5$ K, consistent with a cold, diffuse origin, much like the CO. This temperature agrees within uncertainty with the 27 K found by McCall et al. (2002) toward Cyg OB2 No. 12.

We can infer the size of the cloud from which the H$_3^+$ absorption originates. Using Equation (1), assuming $n_e/n_H =$

Table 5
H$_3^+$ Results

Source	Line ID	Equivalent Width ($\times 10^{-3}$ cm^{-1})	Column Density ($\times 10^{14}$ cm^{-2})
MWC 1080	Q(1,0)	<1.61	<0.6
	R(1,1)^u	<2.43	<1.4
	R(1,0)	<2.36	<0.80
	Total		<1.4
MWC 349	Q(1,0)	2.44 ± 0.3	0.91 ± 0.11
	R(1,1)^u	5.3 ± 0.8	3.0 ± 0.5
	R(1,0)	3.9 ± 0.8	1.3 ± 0.3
	Total		3.9 ± 1.3
	$T_{\rm ex}$		22 ± 5 K
LkHα 101[a]	Q(1,0)	2.8 ± 0.3	1.0 ± 0.1
	R(1,1)^u	2.4 ± 0.3	1.4 ± 0.2
	R(1,0)	2.7 ± 0.3	0.9 ± 0.1
	Total		2.2 ± 0.3
	$T_{\rm ex}$		23 ± 8 K

Note. [a] From Brittain et al. (2004), based on an average of two dates.

1.4×10^{-4} in diffuse clouds (Cardelli et al. 1996), we estimate that a diffuse cloud with a path length of approximately 19 pc, with $n_H \sim 290$ cm^{-3}, is needed to explain the H$_3^+$ absorption. These values are similar to many other lines of sight through the diffuse ISM and in particular are similar to those found toward the Cyg OB association (Indriolo et al. 2007), consistent with MWC 349's location.

4.3. LkHα 101

LkHα 101 is a Herbig Be star, the illuminating source of the NGC 1579 reflection nebula (Herbig 1971). Herbig et al. (2004) inferred a distance of 700 pc to LkHα 101, based on spectroscopic parallaxes for 40 nebulous stars conjectured to lie within the same dark cloud. Visual extinction measurements range from 9.7 to 15.8 mag (Thompson et al. 1976; McGregor et al. 1984; Rudy et al. 1991; Kelly et al. 1994; Herbig et al. 2004). In this paper, we assume that A$_V \sim 10$, as reported by Herbig et al. (2004). Several other B stars, also located in NGC 1579, have measured visual extinctions of 3.5 mag. Those stars and LkHα 101 exhibit diffuse interstellar band (DIB) and interstellar Na I absorption lines in their spectra. The equivalent widths agree toward all sources, including LkHα 101, and are consistent with the 3.5 mag of visual extinction.

However, because of the dense lane of material in front of LkHα 101, it is reasonable to assume that the line of sight extinction is composed of 3.5 mag of the diffuse interstellar material and 6–7 mag of A$_V$ due to the dense lane of material in front of this source (Herbig et al. 2004). This dense material cannot be closer than $\sim$20 pc to LkHα 101 or fluorescent H$_2$ emission should be detected (Brittain et al. 2004). Since the DIB and interstellar Na I features toward LkHα 101 agree with those toward the other objects in NGC 1579, the dense material must be depleted in these carriers. Below, we discuss how our CO and H$_3^+$ observations fit with this characterization of the material along the line of sight to LkHα 101.

4.3.1. CO Toward LkHα 101

The fundamental branches of ^{12}CO and ^{13}CO, as well as the overtone ^{12}CO lines, were observed toward LkHα 101 (see Figures 5–7; Table 4). We found a heliocentric Doppler shift of 6 ± 1 km s^{-1} on 2002 November 15 and 5 ± 1 km s^{-1} on 2003

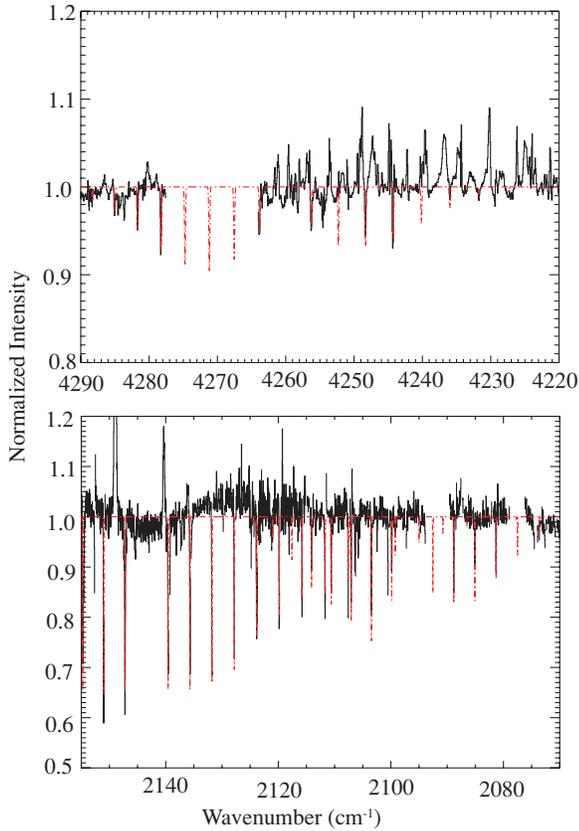**Figure 7.** LkHα 101 residuals with the best-fit collisional model overplotted (red, dashed lines, $N(CO) = 2.3 \times 10^{18}$ cm^{-2}, $T_{rot} = 67$ K, $n_H \geqslant 5 \times 10^6$ cm^{-3}) for the K band (top) and M band (bottom) as discussed in Section 4.3.1. Gaps in the data indicate regions of low transmittance and were eliminated from the analysis. Strong emission lines in both K and M band are due to atomic hydrogen.

(A color version of this figure is available in the online journal.)

March 17. These values agree with the heliocentric Doppler shift of the H$_3^+$ absorption (see below), which would seem to imply that the two molecules originate in the same cloud. However, this is not necessarily the case since the interstellar absorption lines, such as DIBs, toward NGC 1579 also exhibit nearly the same Doppler shift (see Section 4.3; Herbig et al. 2004).

We find that neither the ^{12}CO nor the ^{13}CO fundamental branches are optically thin. We note, for example, that the column densities of the weaker ^{13}CO P-branch lines are larger than those of the R-branch lines, even though the transitions in both branches probe the same rotational state and should yield identical column densities. Similarly, the fundamental ^{12}CO transitions do not yield the same column densities as their overtone counterparts at 2.3 μm. The curve-of-growth analysis resulted in a best-fit Doppler parameter of $b = \sigma_{rms}/1.665 = 0.7 \pm 0.1$ km s^{-1}. This gives the observed ^{12}CO fundamental band P-branch transitions opacities of $\tau \gg 100$ and R-branch overtone transitions $\tau \sim 0.5$–1, so the ^{12}CO column density is $(2.3 \pm 0.2) \times 10^{18}$ cm^{-2}. By applying the best-fit Doppler parameter to the ^{13}CO data, we calculate the line opacities to be $\tau = 1$–4 and yield $N(^{13}CO) = (3.0 \pm 0.4) \times 10^{16}$ cm^{-2}. The resulting $^{12}CO/^{13}CO$ abundance ratio becomes 75 ± 10, comparable to existing millimeter-wave measurements and far less indicative of significant fractionation than suggested by Goto et al. (2003). Applying the collisional model discussed in Section 3.1, we find that a density $\geqslant 5 \times 10^6$ cm^{-3} and rotational

temperature of 67 ± 1 K is needed to fit the CO absorption lines. The resulting model plotted over the ratioed LkHα 101 spectrum is shown in Figure 7.

The CO analysis therefore implies that most of the extinction along the line of sight is due to dense material. Brittain et al. (2004) ran a suite of cloud models that calculated the abundances of important species like H, H$_2$, C$^+$, C, and CO as a function of depth into a cloud (see their Figure 5). These models can account for all of the observed CO seen toward LkHα 101 within A$_V \sim 11$.

However, if there is enough diffuse material along the line of sight to LkHα 101 to provide 3.5 mag of visual extinction, we estimate that the overall CO column density contributed by this material should be approximately 2×10^{14} to 2×10^{16} cm^{-2}, depending on the assumed CO/H$_2$ ratio, or up to 1% of the overall CO. The interstellar DIBs and Na I observed toward NGC 1579 have the same heliocentric Doppler shift as the CO (Herbig et al. 2004; Knappe et al. 1976; Mitchell et al. 1990), so we would not be able to resolve this CO component in our NIRSPEC observations. Hence, we conclude that such a small contribution of CO would be well hidden in our highly saturated CO absorption lines, and the CO analysis does not preclude a contribution from a modest diffuse interstellar cloud toward LkHα 101.

4.3.2. H$_3^+$ Results

Brittain et al. (2004) observed H$_3^+$ toward LkHα 101 and found a total column density of $(2.2 \pm 0.3) \times 10^{14}$ cm^{-2} and a $T_{ex} = 23 \pm 8$ (see Table 5). Can we determine where the H$_3^+$ absorption toward LkHα 101 originates? Brittain et al. (2004) used the relationships above for $N_H/E(B - V)$ and a model for the CO absorption and concluded that the amount of diffuse ISM material along the line of sight was insufficient to account for the observed column density of H$_3^+$. They concluded that the H$_3^+$ absorption arose from the intervening dense material. However, their interpretation depended on an early value for the primary cosmic ray ionization rate of $\sim 2 \times 10^{-17}$ s^{-1}. Recent work has revised the cosmic ray ionization rate in diffuse clouds, making it an order of magnitude higher. This revised value of $\sim 2 \times 10^{-16}$ s^{-1} (Indriolo et al. 2007) may substantially impact the interpretation of H$_3^+$ toward LkHα 101.

Using Equation (1) and solving for L using the earlier cosmic ray ionization rate would imply >100 pc of diffuse cloud material along the line of sight to LkHα 101, an unreasonable amount given the constraints on extinction due to diffuse cloud material toward LkHα 101. Using the revised value in Indriolo et al. (2007) would require a diffuse cloud ~ 11 pc across, which is much more reasonable. If we assume such a cloud were responsible for 3.5 mag of interstellar extinction, we derive an overall n_H of 200 cm^{-3}, consistent with the diffuse cloud densities found by Indriolo et al. (2007). Hence, the observed Doppler shift, H$_3^+$ column density, and the derived hydrogen density, and path length are consistent with enough diffuse material to provide the 3.5 mag of extinction inferred by Herbig et al. (2004).

Can we eliminate a dark cloud origin? The dark lane of material obscuring LkHα 101 provides 6–7 mag of visual extinction, which would imply a molecular hydrogen column density of $\sim 6.7 \times 10^{21}$ cm^{-3}. This is consistent with the CO column density of 2.2×10^{18} cm^{-3} for a standard CO/H$_2$ ratio of $\sim 10^{-4}$. If we assume a cosmic ray ionization rate of 3×10^{-17} s^{-1} for a dark cloud (McCall et al. 1998; Indriolo et al. 2007), we estimate a total path length of ~ 1 pc is

needed to account for the observed H$_3^+$ column density. This is consistent with what has been observed in other dense clouds.

Given our current observations, we cannot conclusively determine where the H$_3^+$ absorption originates. This question can be resolved with further observations. If the H$_3^+$ originates in the diffuse ISM, it should be observable toward the other B stars in the NGC 1579 region that also exhibit 3.5 mag of visual extinction and DIB absorption features. If it originates in the dark lane obscuring LkHα 101, then the other sources in NGC 1579 should not exhibit H$_3^+$ absorption.

5. CONCLUSION

We present results from high-resolution, near-infrared NIRSPEC observations of the fundamental rovibrational CO band from three early-type young stars: MWC 1080, MWC 349, and LkHα 101. We also searched for H$_3^+$ R(1,0), R(1,1)^u and Q(1,0) absorption toward MWC 1080 and MWC 349 and revisited the issue of H$_3^+$ toward LkHα 101 as reported earlier (Brittain et al. 2004).

For MWC 1080, our upper limit on the H$_3^+$ column density implies a minimal amount of diffuse material along the line of sight. This is further supported by the low overall visual extinction (Cohen & Kuhi 1979; Yoshida et al. 1992, $A_V \sim 4$–5). However, we did detect CO in absorption, and our analysis is consistent with the CO located in dense material in the dispersing natal cloud surrounding MWC 1080.

For MWC 349 ($A_V = 8.9$) and LkHα 101 ($A_V \sim 9$–15), we detected H$_3^+$ in absorption. Our analysis is consistent with H$_3^+$ originating in diffuse material along the lines of sight toward both objects. This result is consistent with the results from Indriolo et al. (2007), where they studied H$_3^+$ absorption toward 29 lines of sight through diffuse clouds. In general, H$_3^+$ was detected for any source with $A_V > 5$. For sources with $A_V < 5$, some exhibited substantial column densities of H$_3^+$ and others did not.

CO was detected in absorption toward MWC 349 as well. We found that the H$_3^+$ and CO had the same heliocentric Doppler shift. This suggests that both molecules are located in the same line of sight cloud. The CO was found to not be thermalized so the CO rotational temperature and H$_3^+$ excitation temperature do not agree. However, the data are consistent with both CO and H$_3^+$ located in a diffuse cloud with a path length of $\sim$19 pc.

The line of sight toward LkHα 101 is more complex and probably consists of both diffuse and dense interstellar material. The nearby stars in the same cluster typically have 3.5 mag of visual extinction that result from diffuse interstellar material (Herbig et al. 2004). However, the total extinction toward LkHα 101 has been shown to be nearly 10 mag with the additional 6–7 mag of extinction due to a dark lane of dense cloud material in the foreground. This is in line with our analysis of the CO absorption spectrum, which implies higher density than can be accounted for by diffuse material. The CO results provide a rotational temperature of 67 $\pm$ 1 K for gas in the dark lane, somewhat warmer than typical dense interstellar clouds. The observed column density of material in the diffuse interstellar material is not sufficient to produce much of a contribution to the observed CO. In this analysis, in contrast to reported fractionation from Goto et al. (2003), it was also shown that the ^{12}CO/^{13}CO ratio is 75 $\pm$ 10 which is consistent with current millimeter observations as well as solar system values.

While the bulk of the CO can be shown to reside in the dense material toward LkHα 101, the origin of H$_3^+$ absorption could result from either the diffuse interstellar material or the dark lane. When using the revised diffuse ISM cosmic ray ionization rate found by Indriolo et al. (2007), we can account for the observed H$_3^+$ originating within a diffuse cloud of path length $\sim$11 pc. To resolve this issue will require searching for H$_3^+$ toward the other cluster objects which have better constrained visual extinctions than LkHα 101 and which are not obscured by the dark lane.

REFERENCES

Bohlin, R. C., Savage, B. D., & Drake, J. F. 1978, ApJ, 224, 132
Brittain, S. D., Rettig, T. W., Simon, T., Kulesa, C., DiSanti, M. A., & Dello Russo, N. 2003, ApJ, 588, 535
Brittain, S. D., Simon, T., Kulesa, C., & Rettig, T. W. 2004, ApJ, 606, 911
Cantó, J., Rodríguez, L. F., Calvet, N., & Levreault, R. M. 1984, ApJ, 282, 631
Cardelli, J. A., Meyer, D., M., Jura, M., & Savage, B. D. 1996, ApJ, 467, 334
Cohen, M., Bieging, J. H., Dreher, J. W., & Welch, W. J. 1985, ApJ, 292, 249
Cohen, M., & Kuhi, L. V. 1979, ApJS, 41, 743
DiSanti, M. A., Mumma, M. J., Dello Russo, N., & Magee-Sauer, K. 2001, Icarus, 153, 361
Finkenzeller, U., & Mundt, R. 1984, A&A, 55, 109
Flower, D. R., & Pineau des Forêts, G. 2001, MNRAS, 323, 672
Fuente, A., Martin-Pintado, J., Bachiller, R., Neri, R., & Palla, F. 1998, A&A, 334, 253
Fuente, A., Rodríguez-Franco, A., Testi, L., Natta, A., Bachiller, R., & Neri, R. 2003, ApJ, 598, L39
Geballe, T. R., McCall, B. J., Hinkle, K. H., & Oka, T. 1999, ApJ, 510, 251
Glassgold, A. E., & Langer, W. D. 1974, ApJ, 193, 73
Goorvitch, D., & Chackerian, C., Jr. 1994, ApJS, 91, 483
Goto, M., et al. 2003, ApJ, 598, 1038
Grankin, K. N., et al. 1992, IBVS, 3747, 1
Harvey, P. M., Thronson, H. A., Jr., & Gatley, I. 1979, ApJ, 231, 115
Herbig, G. H. 1971, ApJ, 169, 537
Herbig, G. H., Andrews, S. M., & Dahm, S. E. 2004, AJ, 128, 1233
Herbst, E. 2000, Phil. Trans. R. Soc. A, 358, 2523
Hofmann, K.-H., Balega, Y., Ikhsanov, N. R., Miroshnichenko, A. S., & Weigelt, G. 2002, A&A, 395, 891
Indriolo, N., Geballe, T. R., Oka, T., & McCall, B. J. 2007, ApJ, 671, 1736
Kelly, D. M., Rieke, G. H., & Campbell, B. 1994, ApJ, 425, 231
Knapp, G. R., Kuiper, T. B. H., Knapp, S. L., & Brown, R. L. 1976, ApJ, 206, 443
Kulesa, C. A., & Black, J. H. 2003, in Chemistry as a Diagnostic of Star Formation, ed. C. L. Curry & M. Fich (Ottawa: NRC Press), 60
Kunde, V. R., & Maguire, W. C. 1974, J. Quant. Spectrosc. Radiat. Transfer, 14, 803
Lee, H.-H., Bettens, R. P. A., & Herbst, E. 1996, A&AS, 119, 111
Levreault, R. M. 1985, PhD thesis, Univ. Texas
Levreault, R. M. 1988, ApJS, 67, 283
Lindsay, C. M., & McCall, B. J. 2001, J. Mol. Spectrosc., 210, 60
Mathis, J. S. 1990, ARA&A, 28, 37
McCall, B. J., Geballe, T. R., Hinkle, K. H., & Oka, T. 1998, Science, 279, 1910
McCall, B. J., Geballe, T. R., Hinkle, K. H., & Oka, T. 1999, ApJ, 522, 338
McCall, B. J., et al. 2002, ApJ, 567, 391
McCall, B. J., et al. 2004, Phys. Rev. A, 70, 052716

McGregor, P. J., Persson, S. E., & Cohen, J. G. 1984, ApJ, 286, 609
McLean, I. S., et al. 1998, Proc. SPIE, 3354, 566
Merrill, P. W., & Burwell, C. G. 1949, ApJ, 110, 387
Merril, P. W., Humason, M. L., & Burwell, C. G. 1932, ApJ, 76, 156
Meyer, J. M., Nordsieck, K. H., & Hoffman, J. L. 2002, AJ, 123, 1639
Mitchell, G. F., Maillard, J.-P., Allen, M., Beer, R., & Belcourt, K. 1990, ApJ, 363, 554
Oka, T. 1980, Phys. Rev. Lett., 45, 531
Poetzel, R., Mundt, R., & Ray, T. P. 1992, A&A, 262, 229
Rothman, L. S., et al. 2005, J. Quant. Spectrosc. Radiat. Transfer, 96, 139
Rudy, R. J., Erwin, P., Rossano, G. S., & Puetter, R. C. 1991, ApJ, 383, 344
Savage, B. D., Bohlin, R. C., Drake, J. F., & Budich, W. 1977, ApJ, 216, 291
Schevchenko, V. S., Grankin, K. N., Ibragimov, M. A., Kondratiev, V. B., Melnikov, S. Y. U., Petrov, P. P., Shcherbakov, V. A., & Vitrichenko, L. A. 1994, in ASP Conf. Ser. 62, The Nature and Evolutionary Status of Herbig Ae/Be Stars, ed. P. S. The, M. R. Perez & P. J. Van den Heuvel (San Francisco, CA: ASP), 43

Sheffer, Y., Rogers, M., Federman, S. R., Abel, N. P., Gredel, R., Lambert, D. L., & Shaw, G. 2008, ApJ, 687, 1075
Spitzer, L. 1978, Physical Processes in the Interstellar Medium (New York: Wiley)
Tafoya, D., Gómez, Y., & Rodríguez, L. F. 2004, ApJ, 610, 827
Thompson, R. I., Ericson, E. F., Witteborn, F. C., & Strecker, D. W. 1976, ApJ, 210, L31
van Dishoeck, E. F., & Black, G. A. 1988, ApJ, 334, 771
Wang, S., Looney, L. W., Brandner, W., & Close, L. M. 2008, ApJ, 673, 315
Warin, S., Benayoun, J. J., & Viala, Y. P. 1996, A&A, 308, 535
Wernli, M., Valiron, P., Faure, A., Wiesenfeld, L., Jankowski, P., & Szalewicz, K. 2006, A&A, 446, 367
Yoshida, S., Kogure, T., Nakano, M., Tatematsu, K., & Wiramihardja, S. 1991, PASP, 43, 363
Yoshida, S., Kogure, T., Nakano, M., Tatematsu, K., & Wiramihardja, S. D. 1992, PASP, 44, 77